PERGAMON

Applied Geochemistry 15 (2000) 917–935

Applied Geochemistry

www.elsevier.com/locate/apgeochem

Fluid geochemistry of the Acqui Terme-Visone geothermal area (Piemonte, Italy)

Luigi Marini[a,*], Vittorio Bonaria[a], Massimo Guidi[b], Johannes C. Hunziker[c], Giulio Ottonello[a], Marino Vetuschi Zuccolini[a]

[a]*Dipartimento per lo Studio del Territorio e delle sue Risorse, University of Genova, Corso Europa 26, I-16132 Genova, Italy*
[b]*Istituto di Geocronologia e Geochimica Isotopica, CNR, Via Cardinal Maffi 36, I-56127 Pisa, Italy*
[c]*Université de Lausanne, Institut de Minéralogie et Pétrographie, BFSH-2, CH-1015 Lausanne, Switzerland*

Received 17 November 1998; accepted 4 August 1999
Editorial handling by H. Armannsson

Abstract

The main geothermal reservoir of Acqui Terme-Visone hosts Na–Cl waters, which are in chemical equilibrium at 120–130°C with typical hydrothermal minerals including quartz, albite, K-feldspar, illite, chlorite (or smectite), anhydrite, calcite and an unspecified Ca-Al-silicate. In the Acqui Terme-Visone area, these geothermal waters ascend along zones of high vertical permeability and discharge at the surface almost undiluted or mixed with cold, shallow waters. To the SW of Acqui Terme, other ascending geothermal waters, either undiluted or mixed with low-salinity waters, enter relatively shallow secondary reservoirs, where they reequilibrate at 65–70°C.

Both chemical and isotopic data indicate that bacterial SO_4 reduction affects all these waters, especially those discharged by the secondary reservoirs. Therefore, geothermal waters must get in contact with oil, acquiring the relatively oxidized organic substances needed by SO_4-reducing bacteria. This oil–water interaction process deserves further investigations, for potential economic implications.

1. Introduction

The thermal waters of Acqui Terme and Visone have been known and used therapeutically since Roman times. This is testified by the remnants of the monumental aqueduct, which was built by consul Statilio Tauro during the empire of Augustus (27 B.C.–14 A.D.) to bring cold water to the spas.

In more recent times, the Acqui Terme-Visone area was investigated by means of geological, geochemical and geophysical (geoelectric and seismic methods) surveys to assess its geothermal potential. In particular, results of geochemical investigations have been reported by Dominco et al. (1980) and Bortolami et al. (1983, 1984). Following these surface exploration efforts, a deep geothermal well was drilled at the end of the 1980s. It was a fiasco and brought about the end of geothermal activities in the Acqui Terme-Visone area. However, some shallow wells, which were drilled afterwards for domestic uses, encountered thermal waters, sometimes mixed with cold water.

After almost 10 a, this paper revisits the isotopic and chemical characteristics of the waters discharged at Acqui Terme, through the application of recent geochemical techniques, and formulates an updated

* Corresponding author. Tel.: +39-10-353-8136; fax +39-10-352-169.
E-mail address: luigi@ugo.dipteris.unige.it (L. Marini).

0883-2927/00/$ - see front matter
PII: S0883-2927(99)00094-3

conceptual geochemical model. To achieve these objectives over 50 samples of thermal and cold water discharges were collected and analyzed both chemically and isotopically. The authors hope that these new findings may stimulate a new interest in the evaluation and exploitation of the natural resources of the study area.

A section of the paper discusses the chemical and isotopic evidence supporting the occurrence of bacterial reduction of SO_4 to sulfide, accompanied by oxidation of organic substances to carbonate species. The thermal waters of Acqui Terme and Visone provide a clear example of this important process, which deserves further attention for potential economic implications.

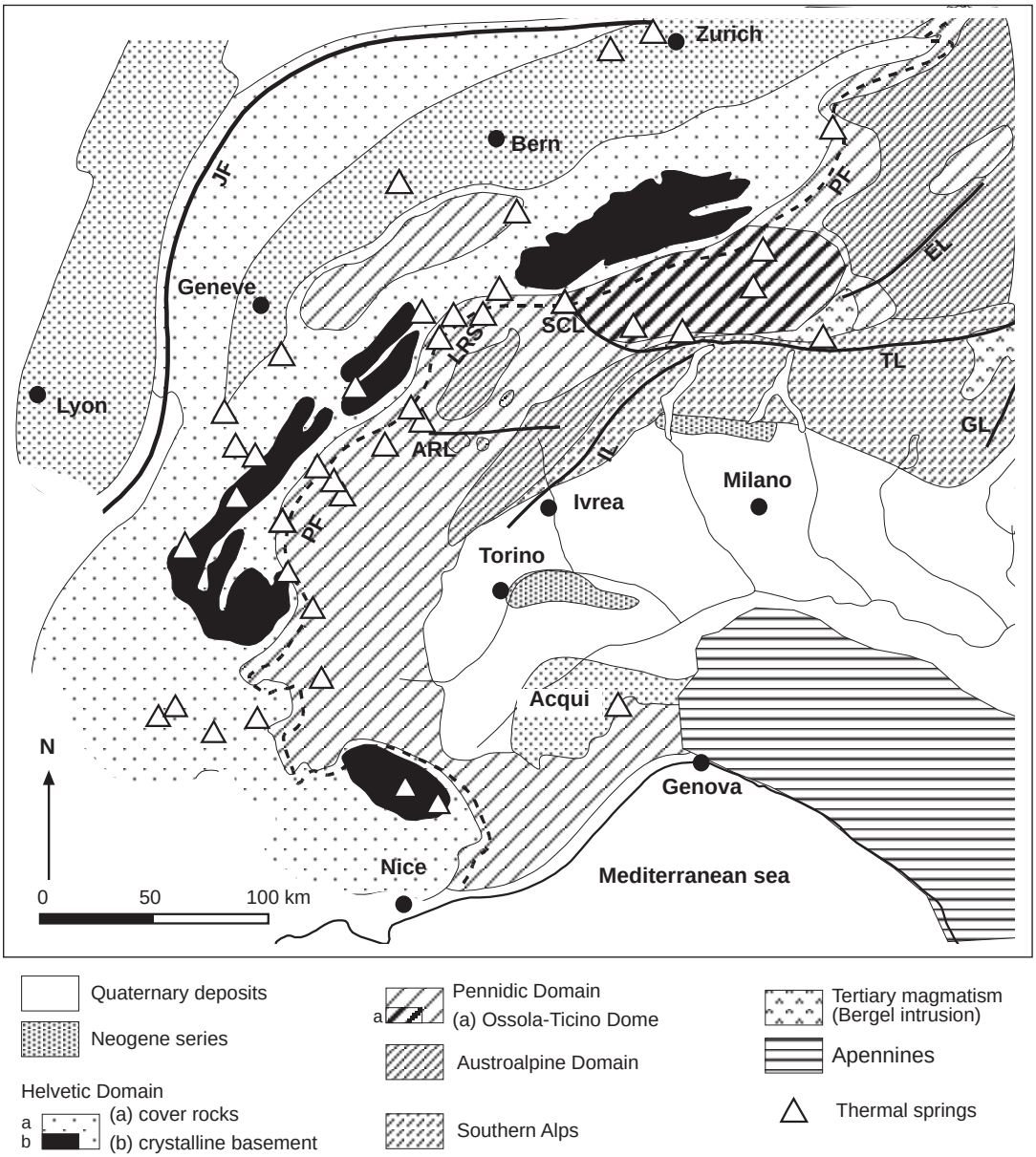

Fig. 1. Locations of main thermal springs (triangles) in the western Alps (from Perello, 1997). PF = Pennidic Front; JF = Giura Front; SCL = Simplon-Centovalli Line; RSL = Rhone-Simplon Line; EL = Engadina Line; TL = Tonale Line; ARL = Aosta-Ranzola Line; GL = Giudicarie Line.

2. Geological framework

As recognized by Perello (1997, and references therein) most thermal springs of the western Alps are located external to the mountain chain and close to two regional lithospheric discontinuities, which have been tectonically active until present: (1) the Pennidic Front, a ductile deformation zone reactivated by brittle shearing during late Neogene, and (2) the Rhone-Simplon shear zone (Fig. 1). The thermal area of Acqui Terme-Visone is the only one located in the inner sector of the western Alps, but in a peculiar situation that is comparatively close to the Alps–Apennines boundary.

In a close-up view, the thermal area of Acqui Terme-Visone is located in an E–W trending sector of the Bormida valley, where the mainly marine sedimentary rocks of the Tertiary Piemonte Basin (TPB for short, Lower Oligocene–Lower Pliocene) outcrop. This sequence includes the gypsum-bearing evaporites of Messinian age that are exposed north of Acqui Terme. To the south of Acqui Terme, the transgressing marine sediments of the TPB unconformably overlie the inner sector of the Ligurian Alpine edifice. The latter largely consists of: (1) ophiolites (mainly serpentinites, gabbros and ultramafic rocks) and related marine metasedimentary rocks (chiefly calc-schists and quartz-schists) of the Voltri Group (Chiesa et al., 1975; Capponi et al., 1994) and (2) mainly carbonate rocks of Triassic–Jurassic age, including Upper Triassic evaporites, as observed in the Sestri-Voltaggio area (Cortesogno and Haccard, 1984). Locally, metamorphic and crystalline rocks, such as those of the Valosio Massif (paragneiss, orthogneiss, garnet-mica-schists, amphibolites, silicate-bearing marbles; Cabella et al., 1991), also make up the Ligurian Alpine edifice.

In the absence of direct observations, hints of the rocks actually present below the marine sediments of the TPB at Acqui Terme are provided by geophysical data and regional geological models. According to Cassano et al. (1986), an anomaly of high magnetic susceptibility, possibly related to buried ophiolites, is present in a wide sector of southern Piemonte including Acqui Terme. Regional geological models indicate that the ultramafic rocks, serpentinites and metasediments of the Voltri Group as well as the carbonate rocks of Triassic–Jurassic age (including Upper Triassic evaporites) underlie Acqui Terme (Cassano et al., 1986; Biella et al., 1988; Piana et al., 1997). The marine sediments of the TPB, as a whole, represent an impermeable sequence, whose thickness is approximately 2–3 km in the study area. Nevertheless this seal is locally inefficient and comparatively high fluxes of ascending thermal waters go through it, such as in the Acqui Terme-Visone area. The upflow of these thermal waters is locally permitted by conditions of high vertical permeability, which are governed by the NW- to W-trending normal and strike–slip faults belonging to the transtensive Bagni-Visone fault system (Piana et al., 1997).

3. Field work, laboratory analyses and data presentation

Sample locations are shown in Fig. 2. Field characteristics are given in Appendix A for the most important thermal and mineral springs and wells only.

In February 1997, 45 water samples were collected from different sites, comprising springs and shallow wells. The main thermal manifestations and 5 new sites (labelled 46 to 50) were sampled again in June 1997. Repeated samples are identified by the same codes of the first survey followed by the letter b.

Outlet temperature, pH, Eh, alkalinity (acidimetric titration) and sulfide (methylene blue colorimetric method) were determined in the field. Raw, filtered (0.45 μm) and filtered-acidified (with HCl 1:1) samples were collected and stored in polyethylene bottles, from each sample-site, for the analysis of major dissolved species, some minor constituents and the $^{2}H/^{1}H$ and $^{18}O/^{16}O$ isotope ratios. Water samples were chemically analyzed in the laboratory of the Institute of Geochronology and Isotope Geochemistry, CNR, Pisa, Italy as follows:

- Li, Na, K, Mg, Ca by atomic absorption spectrophotometry and/or atomic emission spectrophotometry,
- Cl, SO_4, NO_3 by ion chromatography,
- B, SiO_2 by visible spectrophotometry,
- F by ionselective electrode.

The $^{2}H/^{1}H$ and $^{18}O/^{16}O$ isotope ratios of 24 selected samples were determined at the Institut de Minéralogie et Pétrographie of Lausanne University, Switzerland by means of a Finnigan MAT 251 mass spectrometer, which is calibrated with an internal standard. This, in turn, is calibrated against SMOW and SLAP international reference materials and GISP intercalibration material following the recommendation of Coplen (1988). Deviation of the intralaboratory INHOUSE standard is $\pm 1‰$ for δD and $\pm 0.05‰$ for $\delta^{18}O$.

All the analytical results are given in Table 1, together with total carbonate and total ionic salinity. Total carbonate (TC) represents the sum of the molal concentrations of $CO_{2,aq}$, HCO_3^-, CO_3^{2-}, and related aqueous complexes and was computed through speciation calculations carried out by means of SOLVEQ (Reed and Spycher, 1984). These calculations are largely based on pH and titration (total) alkalinity and take into account the contributions of inorganic acid

anions (such as $H_3SiO_4^-$, $H_2BO_3^-$, etc.), but neglect the contributions of organic acid anions (such as formate, acetate, propanoate, oxalate, etc.). Therefore, total carbonate may be overestimated for waters rich in organic acid anions, which is the case for some oil field waters (Wiley et al., 1975). Ionic salinity, Σeq, is defined as follows (Chiodini et al., 1991):

$$\Sigma\mathrm{eq} = \Sigma|z_i|m_i, \quad (1)$$

where z_i and m_i are the ionic charge and the molality of the ith species, respectively.

The $^{34}S/^{32}S$ isotope ratio of dissolved SO_4 was determined in 4 selected samples and of dissolved sulfide in one sample at the laboratory of the Institute of Geological and Nuclear Sciences, Lower Hutt, New Zealand. In the field, 1 kg of water was acidified to pH 1.5 with HCl and treated with $CuCl_2$, to precipitate sulfide as CuS. In the laboratory, solid CuS was separated through filtration from the aqueous solution and the latter was heated and treated with $BaCl_2$, to precipitate SO_4 as $BaSO_4$. An amount of CuS sufficient for the determination of the $^{34}S/^{32}S$ isotope ratios was obtained

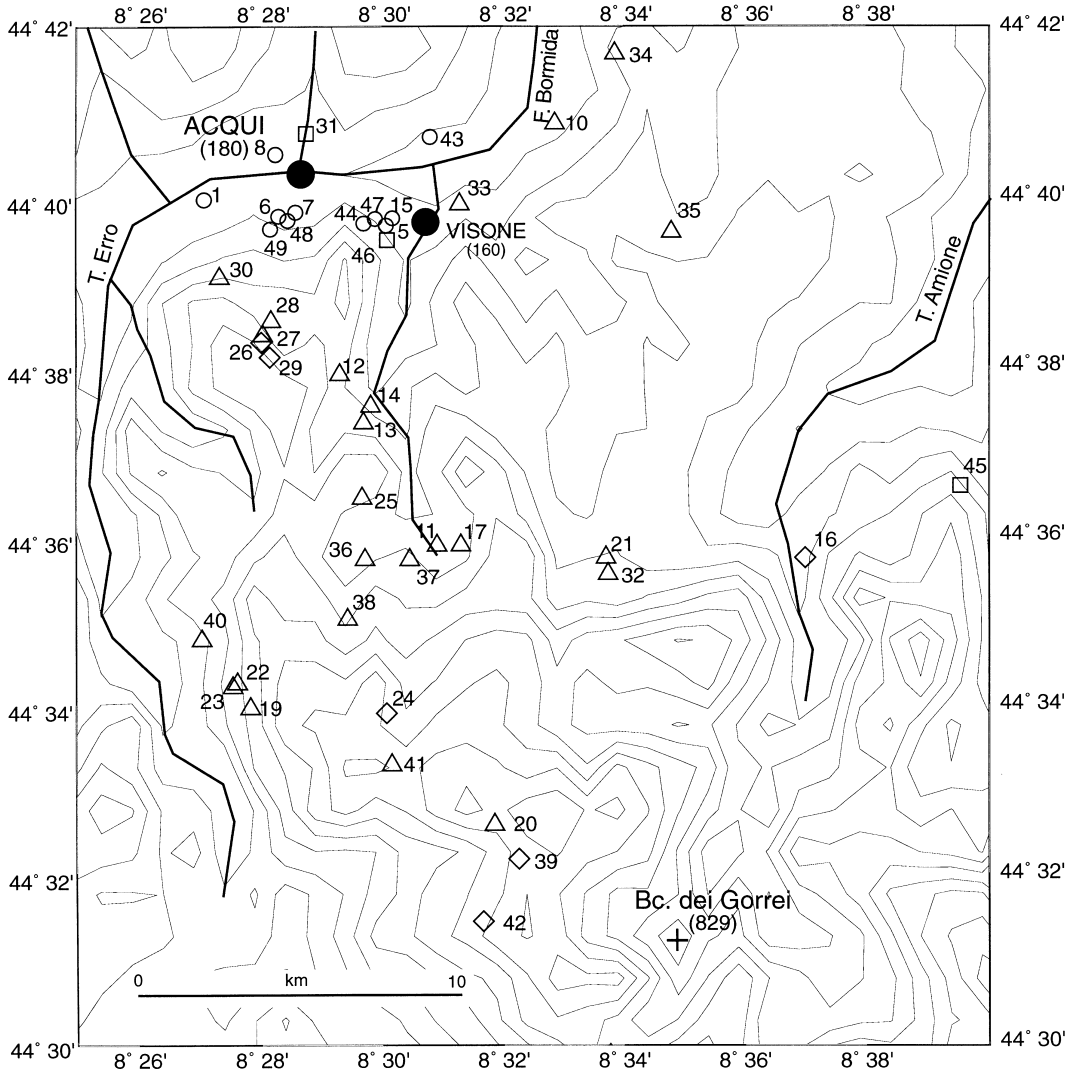

Fig. 2. Map of the study area showing the location of most samples collected in February and June 1997. (○) Na–Cl waters; (□) Na-HCO_3 waters; (△) Ca–HCO_3 waters; (◇) Mg–HCO_3 waters. Also shown is the topographic relief (thin lines; contours every 100 m) and the stream network (heavy lines). Coordinates of outliers are as follows: Code 2: 44°43′44″N8°28′08″E; Code 3: 44°49′40″N8°52′09″E; Code 4: 44°45′52″N8°36′05″E; Code 9; 44°42′15″N8°34′11″E; Code 18: 44°29′57″N8°33′45″E; Code 50: 44°21′26″N8°26′43″E

Table 1
Chemical data, δD and $\delta^{18}O$ values for waters circulating in the Acqui Terme-Visone area. Total (titration) alkalinity (Alk) is in mg/kg HCO_3. Total carbonate (TC) represents the sum of the molal concentrations of $CO_{2,aq}$, HCO_3^-, CO_3^{2-}, and related aqueous complexes and was computed through speciation calculations carried out by means of SOLVEQ (Reed and Spycher, 1984). Σeq stands for ionic salinity. n.d. = not detected; n.a. = not analyzed

Code	T (°C)	Eh (mV)	Ph	Li (ppm)	Na (ppm)	K (ppm)	Mg (ppm)	Ca (ppm)	Alk (ppm)	TC (mmol/kg)	SO_4 (ppm)	Cl (ppm)	F (ppm)	NO_3 (ppm)	HS (ppm)	SiO_2 (ppm)	B (ppm)	Σeq (meq/kg)	δD (‰ vs SMOW)	$\delta^{18}O$
1	25.7	−220	7.77	0.49	435	6.75	4.87	35.2	257	4.29	76.1	609	6.8	n.d.	9.0	25.6	3.6	44.6	n.a.	n.a.
2	14.6	+73	6.90	0.055	19.4	4.64	65.3	623	425	8.54	1420	26.3	n.d.	n.d.	n.d.	18.8	0.13	74.7	n.a.	n.a.
3	15.1	+138	7.72	n.d.	11.5	1.00	24.4	42.5	269	4.58	7.99	5.45	n.d.	2.11	n.d.	28.9	0.06	9.4	n.a.	n.a.
4	12.2	+105	7.50	n.d.	9.55	0.76	19.2	70.9	277	4.86	25.2	16.4	n.d.	11.5	n.d.	15.6	n.d.	11.3	n.a.	n.a.
5	21.8	+89	7.54	1.10	561	13.0	4.03	135	89	1.52	204	948	5.4	n.d.	n.d.	44.0	6.3	64.5	n.a.	n.a.
6	38.8	n.a.	7.73	1.34	704	14.8	0.21	142	17	0.24	231	1160	6.6	0.64	0.08	52.3	7.7	76.3	n.a.	n.a.
7	34.8	−150	8.32	1.31	685	14.7	0.54	140	27	0.25	228	1180	6.7	n.d.	2.0	48.9	7.5	76.0	n.a.	n.a.
8	69.5	−154	8.04	1.29	665	14.1	0.16	135	23	0.16	230	1130	6.8	n.d.	1.5	52.6	7.3	73.4	n.a.	n.a.
9	13.8	+34	7.08	0.035	12.5	3.93	63.3	132	474	9.14	222	8.14	n.d.	n.d.	n.d.	37.2	0.10	25.1	n.a.	n.a.
10	12.4	+172	6.85	0.016	12.7	3.04	27.0	175	502	10.7	73.2	30.5	n.d.	50.2	n.d.	19.4	0.08	23.0	n.a.	n.a.
11	10.9	+175	7.52	n.d.	4.48	1.82	35.4	59.8	342	5.99	19.2	3.89	n.d.	3.39	n.d.	12.1	n.d.	12.3	−58.4	−8.64
12	12.5	+72	7.29	0.010	8.16	1.18	37.4	93.3	378	6.90	88.7	8.12	n.d.	0.42	n.d.	18.1	n.d.	16.4	−58.9	−8.92
13	9.6	+210	7.32	n.d.	3.41	0.42	33.4	68.6	331	6.04	35.4	5.05	n.d.	12.8	n.d.	14.2	n.d.	12.8	n.a.	n.a.
14	11.3	+235	7.45	n.d.	4.22	0.56	27.9	77.1	297	5.26	67.1	5.63	n.d.	2.98	n.d.	20.4	n.d.	12.8	n.a.	n.a.
15	11.4	+185	7.11	0.43	229	4.50	12.5	102	233	4.47	122	390	2.2	15.4	n.d.	24.8	2.7	33.9	n.a.	n.a.
16	11.8	+145	7.80	n.d.	6.22	1.06	68.5	32.5	370	6.26	74.8	6.45	n.d.	1.22	n.d.	41.3	n.d.	15.4	n.a.	n.a.
17	10.2	+225	7.70	n.d.	4.72	1.17	34.7	63.1	322	5.51	32.5	7.15	n.d.	16.6	n.d.	10.0	n.d.	12.7	n.a.	n.a.
18	8.4	+178	7.25	n.d.	2.55	0.36	1.04	18.2	56	1.05	2.19	3.78	n.d.	0.05	n.d.	8.4	n.d.	2.2	−59.0	−8.18
19	9.0	+235	8.16	n.d.	2.90	0.84	5.67	52.3	168	2.78	17.3	8.01	n.d.	1.16	n.d.	8.6	n.d.	6.6	n.a.	n.a.
20	7.7	+214	7.67	n.d.	6.06	0.82	2.27	26.1	87	1.51	8.19	4.92	n.d.	n.d.	n.d.	15.2	n.d.	3.5	−61.0	−9.02
21	10.5	+15	7.38	0.017	5.65	0.58	24.6	95.6	311	5.58	95.5	4.17	n.d.	n.d.	n.d.	26.6	n.d.	14.3	n.a.	n.a.
22	9.0	+65	7.20	0.011	5.45	1.47	20.7	109	361	6.80	70.8	6.13	n.d.	n.d.	n.d.	12.0	n.d.	15.0	n.a.	n.a.
23	9.5	+180	7.15	0.011	4.74	1.44	24.6	129	382	7.29	67.3	3.11	n.d.	2.40	n.d.	14.1	n.d.	16.5	n.a.	n.a.
24	8.7	+240	6.87	n.d.	4.66	1.31	17.6	12.6	119	2.63	12.2	5.04	n.d.	6.13	n.d.	19.3	n.d.	4.8	−62.0	−8.84
25	9.0	+230	7.61	n.d.	5.08	0.52	9.36	85.9	260	4.51	31.4	5.89	n.d.	7.30	n.d.	9.4	n.d.	10.5	−59.8	−8.57
26	15.2	+47	7.45	0.030	19.9	4.15	42.8	58.5	364	6.42	65.0	10.9	n.d.	0.53	n.d.	15.5	0.06	15.0	n.a.	n.a.
27	13.2	+225	7.35	n.d.	5.10	1.84	26.8	110	365	6.56	103	5.28	n.d.	1.30	n.d.	12.5	n.d.	16.3	−60.7	−8.73
28	17.4	+230	7.46	0.032	35.1	4.54	11.6	87.5	315	5.53	73.0	7.49	n.d.	7.87	n.d.	9.9	0.12	14.0	n.a.	n.a.
29	18.7	+155	7.58	0.037	40.3	3.33	37.1	49.7	391	6.74	46.5	4.52	n.d.	1.65	n.d.	17.6	0.09	14.9	n.a.	n.a.
30	11.7	+235	7.37	0.015	11.0	6.16	21.9	119	341	6.12	82.7	28.1	n.d.	34.6	n.d.	14.3	n.d.	17.0	n.a.	n.a.
31	30.1	+185	7.38	0.10	188	5.14	40.0	46.8	476	8.37	273	47.8	n.d.	3.68	n.d.	22.5	1.0	28.8	n.a.	n.a.
32	11.0	+165	7.38	0.012	3.31	0.40	27.4	91.0	255	4.58	135	3.77	n.d.	0.52	n.d.	24.7	n.d.	14.1	−59.7	−8.25
33	11.3	+247	7.07	0.028	27.9	2.34	49.5	143	469	9.13	176	36.4	n.d.	9.38	n.d.	24.7	n.d.	25.0	−58.6	−8.33
34	11.0	+190	7.18	n.d.	7.45	2.96	29.3	132	440	8.28	65.0	12.5	n.d.	33.7	n.d.	16.5	n.d.	18.9	n.a.	n.a.
35	10.9	+280	7.19	0.02	3.74	2.03	23.9	118	399	7.50	61.8	4.76	n.d.	2.60	n.d.	28.2	n.d.	16.1	n.a.	n.a.
36	9.4	+278	6.92	n.d.	3.25	0.28	23.3	45.8	221	4.69	22.3	3.53	n.d.	6.79	n.d.	18.0	n.d.	8.6	n.a.	n.a.
37	7.6	+243	7.54	n.d.	5.93	0.17	12.4	44.1	187	3.29	10.2	3.76	n.d.	1.82	n.d.	9.7	n.d.	6.9	n.a.	n.a.
38	10.0	+287	7.51	n.d.	5.18	0.45	32.0	64.8	310	5.44	29.1	6.00	n.d.	9.89	n.d.	24.0	n.d.	12.1	−57.4	−8.94
39	7.3	+252	7.43	n.d.	5.29	0.30	26.0	14.4	154	2.76	10.5	7.88	n.d.	8.98	n.d.	30.3	n.d.	6.2	−59.5	−9.25
40	13.7	+267	7.55	0.009	4.17	2.13	23.9	104	348	6.05	52.0	11.1	n.d.	9.31	n.d.	13.9	n.d.	14.6	−61.2	−9.05
41	6.0	+270	7.20	n.d.	7.64	0.27	26.2	51.8	246	4.69	15.9	20.9	n.d.	1.48	n.d.	18.0	n.d.	10.1	n.a.	n.a.
42	9.2	+255	8.23	n.d.	1.80	0.18	33.2	19.9	211	3.47	8.1	4.22	n.d.	2.09	n.d.	37.9	n.d.	7.6	−64.5	−9.02
43	13.7	−55	7.58	0.22	4620	25.8	196	425	85	1.40	4.3	8895	1.0	n.d.	n.d.	13.4	16.8	491.4	−47.3	−5.58
44	31.9	−40	8.73	0.92	501	8.82	0.23	78.7	26	0.16	171	767	7.6	n.d.	0.5	28.4	6.4	52.0	n.a.	n.a.
45	11.0	−25	7.53	0.046	105	8.62	25.20	60.3	348	6.08	105	71.4	n.d.	n.d.	0.6	20.4	0.29	19.8	n.a.	n.a.
46	32.0	+33	8.62	0.23	142	1.90	0.14	7.30	127	1.99	78.1	80.5	12	n.d.	n.d.	20.0	n.d.	13.2	n.a.	n.a.
47	23.0	−130	7.67	1.10	561	12.4	4.22	133	101	1.68	196	928	4.7	n.d.	1.3	42.8	6.4	63.9	−65.5	−9.01
48	42.5	−33	7.98	1.36	695	14.7	0.20	143	21	0.25	226	1170	5.8	n.d.	0.01	49.8	7.8	76.1	−67.4	−8.29
49	18.0	−250	7.58	0.74	840	11.5	17.5	74.2	247	4.21	80.1	1340	5.4	n.d.	31.0	28.3	5.5	85.8	−68.3	−9.49
50	14.5	n.a.	8.55	0.10	113	3.20	16.0	10.0	363	5.86	25.1	11.0	n.d.	n.d.	0.08	19.4	0.42	13.6	−82.8	−11.64
1b	26.0	−255	7.76	0.49	435	6.43	5.09	36.3	256	4.29	60.0	586	6.2	n.d.	17.0	23.9	3.7	43.6	−69.3	−9.75
5b	21.5	−63	7.58	1.09	563	12.4	4.12	135	91	1.54	192	940	4.5	n.d.	0.02	41.9	6.2	64.1	−64.6	−9.07
6b	40.0	−5	7.87	1.34	703	14.6	0.21	143	19	0.24	223	1175	6.2	n.d.	0.06	48.4	7.8	76.5	−66.9	−8.51
7b	36.0	−190	8.32	1.33	686	14.4	0.41	140	29	0.27	222	1180	5.7	n.d.	1.0	46.2	7.7	75.9	n.a.	n.a.
8b	69.5	−155	8.16	1.30	661	14.0	0.14	136	28	0.24	220	1120	5.8	n.d.	0.27	49.6	7.4	72.9	−68.2	−9.05
15b	13.3	+109	7.04	0.72	388	7.15	8.53	107	153	2.99	152	619	3.2	2.90	n.d.	27.4	4.4	46.5	−61.7	−8.81
44b	31.5	−113	8.65	0.94	494	8.78	0.22	81.8	29	0.25	167	772	6.6	n.d.	0.16	27.4	6.5	51.9	−66.6	−9.26

for sample 1b only. The reproducibility of $^{34}S/^{32}S$ isotope ratios is ±0.2‰. Results are presented and discussed in the Section on bacterial SO_4 reduction.

Tritium activity of sample 1b, 0.0 ± 0.3 T.U., was determined in the laboratory of the International Institute for Geothermal Research, CNR, Pisa, using a proportional gas counter after eletrolytic enrichment and conversion of H_2 to C_2H_6.

4. Water composition and preliminary constraints on origins

The chemical composition of the waters sampled in the Acqui Terme-Visone area is described in terms of relative Cl, SO_4 and HCO_3 concentrations (Fig. 3, after Giggenbach, 1988) and relative Na + K, Ca and Mg contents (Fig. 4). Previous data by Dominco et al. (1980) and Bortolami et al. (1983, 1984) are also shown in these diagrams. Inspection of these triangular plots points to the occurrence of the following types of waters.

4.1. Ca–HCO_3 to Mg–HCO_3 waters of low salinity

This group includes 34 samples, numbered 3, 4, 9 to 14, 16 to 30 and 32 to 42. All these waters are characterized by low ionic salinities, 2–25 meq/kg. Chloride contents are generally low, 3–12 mg/kg, although 5 samples have Cl concentrations of 16–36 mg/kg, possibly due to pollution. The springs of this group have temperatures of 6–14°C, which are close to the average annual air temperature at the discharge elevation, indicating that these waters come from shallow, short-lived hydrogeological circuits. The chemical and physical characteristics of these Ca–HCO_3 to Mg–HCO_3 waters are typical of the first stages of interaction between meteoric waters and rocks (including soils). Compositional differences are due to interaction with different lithotypes.

Meteoric waters acquire saturation with calcite and Ca–HCO_3 composition in the initial stages of interaction with rocks containing even small amounts of calcite (Freeze and Cherry, 1979). The reason for this is that, at temperatures close to 25°C, the dissolution rate of calcite is 2 to 6 orders of magnitude higher than that of Al-silicates, depending upon the pH (Stumm and Morgan, 1996 and references therein).

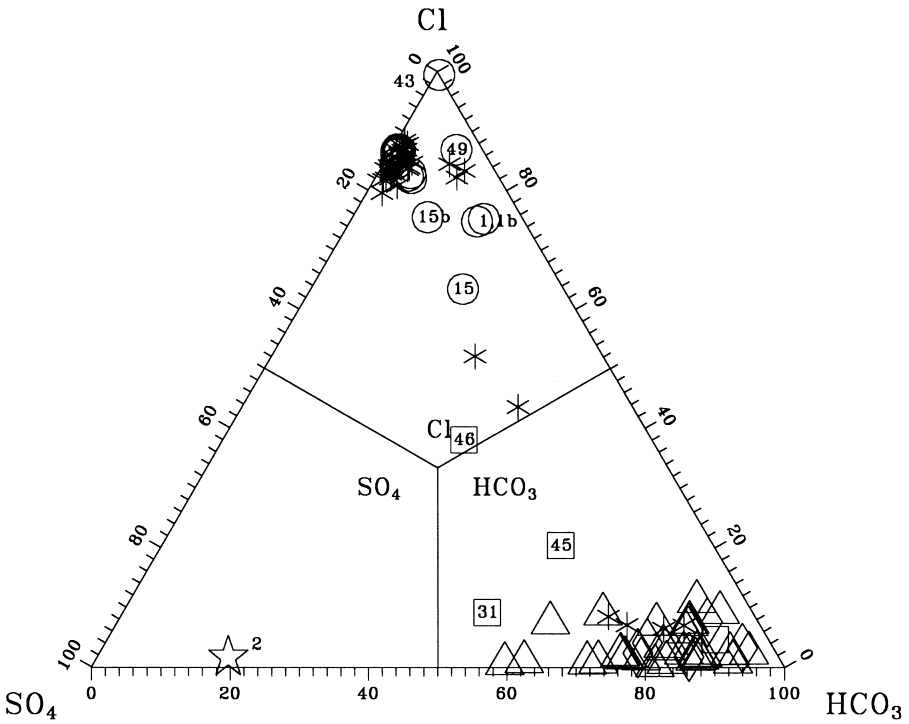

Fig. 3. Relative Cl, SO_4 and HCO_3 concentrations, in equivalents, of the waters of the study area (adapted from Giggenbach, 1988). (○) Na–Cl waters; (□) Na–HCO_3 waters; (△) Ca–HCO_3 waters; (◇) Mg–HCO_3 waters; (☆) Ca–SO_4 waters; (∗) samples of Dominco et al. (1980) and Bortolami et al. (1983, 1984).

Meteoric waters acquire Mg–HCO_3 composition through interaction with ultramafic rocks (Barnes et al., 1967, 1978; Barnes and O'Neil, 1971). The prevalence of Mg among the dissolved cations is consistent with the chemical and mineralogical characteristics of these rocks and with the high dissolution rates of the minerals involved. Magnesium–HCO_3 waters have been encountered in the Polcevera valley, near Genova, where the ophiolites of the Voltri Group outcrop (Marini and Ottonello, 1997).

In the study area, Mg–HCO_3 waters originate through leaching of the ophiolites of the Voltri Group, Ca–HCO_3 waters form by interaction of meteoric waters with calcite-bearing sedimentary rocks lacking in ophiolitic clasts and Ca–Mg–HCO_3 waters come from interaction with either calcite-bearing sedimentary rocks and ophiolites or the Molare Formation, which includes conglomerates and sandstones with clasts of ophiolites.

4.2. Na–HCO_3 waters of low salinity

This group comprises samples 31, 45, 46 and 50, which have ionic salinities of 10–30 meq/kg, i.e., comparable to those of cold Ca–HCO_3 to Mg–HCO_3 waters. However Cl concentrations of the Na–HCO_3 waters (up to 81 mg/kg in sample 46) are higher than those of Ca–HCO_3 to Mg–HCO_3 waters, except sample 50, whose Cl concentration is only 11 mg/kg. Samples 45 and 50 have detectable sulfide. The temperatures of these two waters are close to the average annual air temperature whereas temperatures of waters 31 and 46 (30.1 and 32.0°C, respectively) are significantly higher than average annual air temperature. Simple Cl and enthalpy balances show that the anomalous high temperatures of these two waters, which are located close to zones of ascent and discharge of thermal waters, cannot be explained by mixing of thermal waters with cold Ca–HCO_3 to Mg–HCO_3 waters. Therefore, they are heated by either input of hot gases from below or, most likely, conductive heat transfer.

In high-enthalpy geothermal areas, Na–HCO_3 waters originate through either absorption of CO_2-bearing gases or condensation of CO_2-rich geothermal steam in O_2-free, low-salinity waters of shallow circulation (e.g., Mahon et al., 1980; Giggenbach, 1988). As the absence of O_2 prevents oxidation of H_2S to H_2SO_4, the acidity of these waters is controlled by H_2CO_3. These H_2CO_3-rich waters convert feldspars to clays, thus evolving towards a Na–HCO_3 composition. The aqueous solution becomes rich in Na and HCO_3 as Ca and SO_4 concentrations are limited by the low solubility of calcite and anhydrite, respectively, and K and Mg are taken up in clays (Ellis and Mahon, 1977).

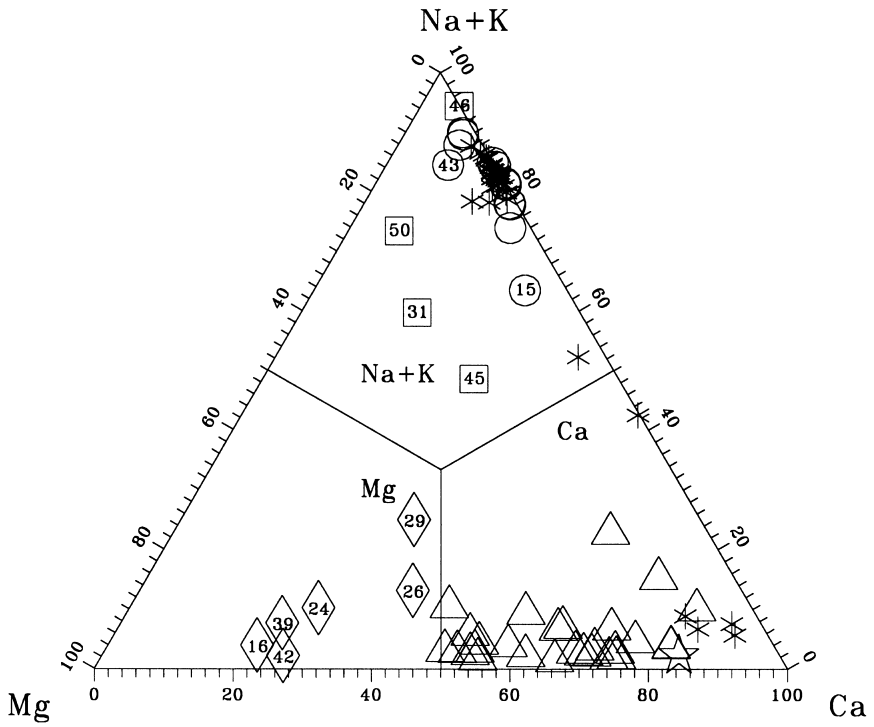

Fig. 4. Relative Na + K, Ca and Mg concentrations, in equivalents, of the waters of the study area. Symbols as in Fig. 3.

Conversion of feldspars to clays probably controls the chemistry of natural waters from the initial Ca–HCO_3 facies towards the final Na–HCO_3 composition also in low-temperature systems. A necessary condition for this evolution is the absence of SO_4 and Cl sources, mainly evaporites. Pastorelli (1999) simulated this process by reacting a Ca–HCO_3 water with a gneissic rock, bearing both K-feldspar and plagioclase, at 25°C and variable P_{CO_2}, by means of the EQ3NR-EQ6 Software Package, version 7.2 (Wolery and Daveler, 1992; Wolery, 1992). The P_{CO_2} was decreased step-wise from $10^{-2.76}$ bar, the value of the Ca–HCO_3 water, to $10^{-4.05}$ bar, the value of the Na–HCO_3 water. The simulation was carried out in reaction progress mode following the titration model (Wolery and Daveler, 1992). Kaolinite, muscovite, K-feldspar, quartz, dolomite and calcite were precipitated during water–rock interaction. The analytical concentrations of Na, K, Mg, Ca, C, S, Cl and F, and the pH of the Na–HCO_3 water were reproduced within analytical uncertainties for a reaction progress of 0.2 moles.

Based on these findings it can be concluded that, also in the study area, prolonged interaction of meteoric waters with clastic rocks, bearing both K-feldspar and plagioclase, is the process likely to control the origin of Na–HCO_3 waters, whose times of circulation and water–rock interaction are greater than those of cold Ca–HCO_3 to Mg–HCO_3 waters, as suggested also by the comparatively high Cl contents.

An alternative process producing Na–HCO_3 waters is the cation exchange of Na^+ for Ca^{2+} from Ca–HCO_3 waters (e.g., Appelo, 1996 and references therein). This mechanism was proposed to explain the origin of the Na–HCO_3 waters discharged by Tertiary aquifers along the coast of western Europe and eastern North America. In the study area it is difficult to establish the role of this process as the exchange properties of local rocks are poorly known.

4.3. Ca–SO_4 waters of high salinity

The only Ca–SO_4 water is sample 2, which is from a shallow well, a few km north of Acqui Terme. This sample has a high ionic salinity, 75 meq/kg, and a low temperature, 14.6°C, which is only slightly higher than the average annual air temperature. This sample is likely to be an example of the Ca–SO_4 waters which are relatively common in the Po plain. Their characteristics are due to interaction with the gypsum-bearing evaporites of Messinian age (Bortolami et al., 1984).

The high SO_4 content (>100 mg/kg) of some Ca–HCO_3 waters in the study area (i.e., samples 9, 27, 32 and 33) is attributed to mixing of low-salinity, Ca–HCO_3 waters with small amounts of high-salinity Ca–SO_4 waters.

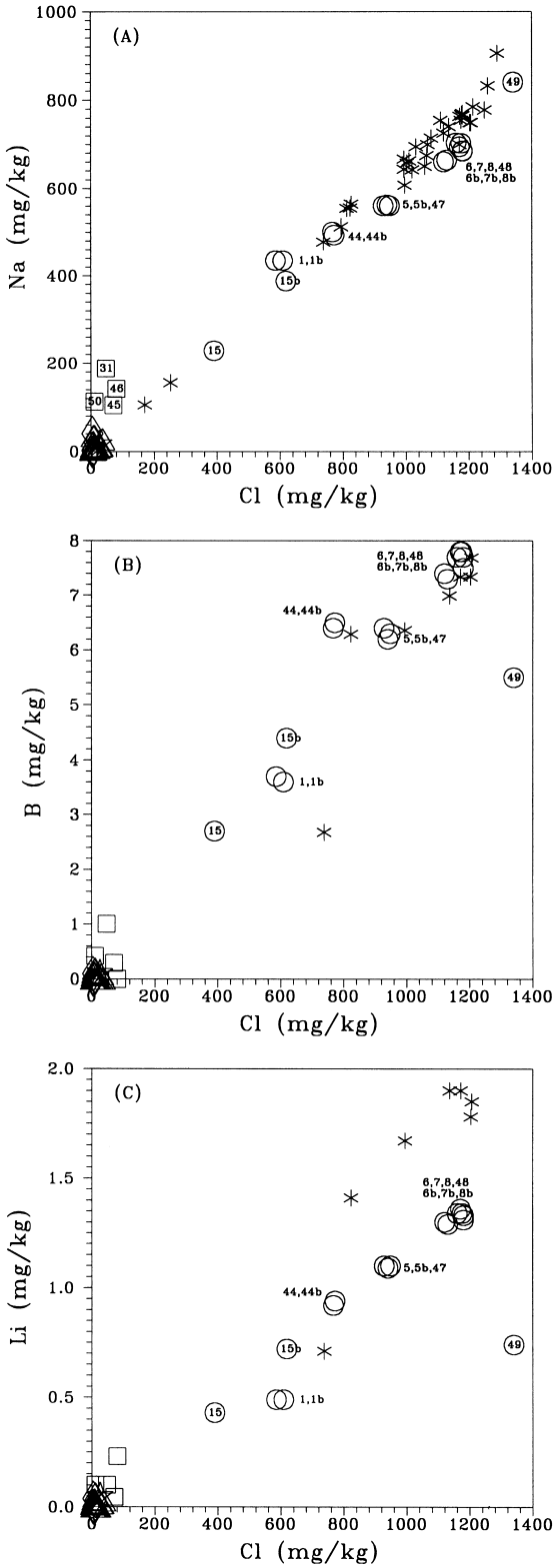

Fig. 5. (A): Na vs. Cl plot. (B): B vs. Cl plot. (C): Li vs. Cl plot. Symbols as in Fig. 3.

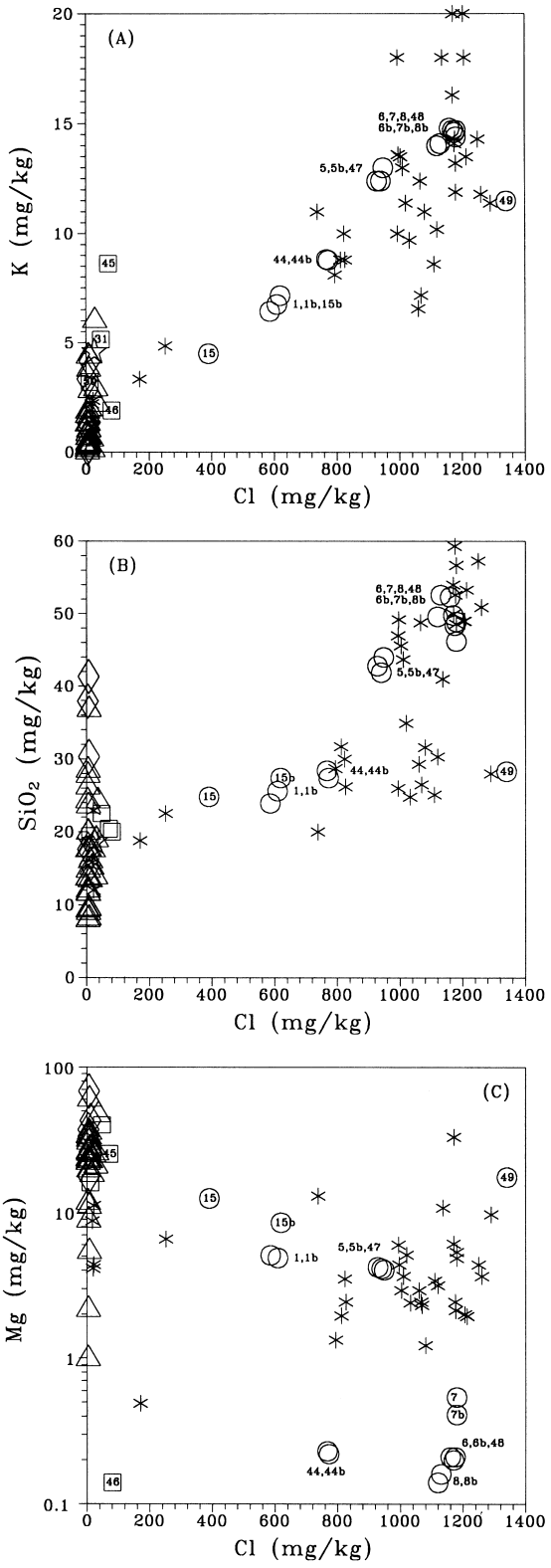

Fig. 6. (A): K vs. Cl plot. (B): SiO_2 vs. Cl plot. (C): Mg vs. Cl plot. Symbols as in Fig. 3.

4.4. Na–Cl waters of high salinity

The only Na–Cl water of high salinity is from the Cascina Corsina well, sample 43. It has a temperature of 13.7°C and a very high ionic salinity, ~500 meq/kg. Chloride, with a concentration of 8895 mg/kg, is the predominant anion, while Na, with a concentration of 4620 mg/kg, is the dominant cation. These waters, which are not uncommon in the Po plain, have a marine origin (e.g., dilution of connate marine water or interaction of groundwaters with the residues of evaporated seawater, known as "bitterns"), as pointed out by Bortolami et al. (1984 and references therein). Consistent with this origin, the Na/Cl wt ratio of sample 43, 0.519, is only slightly lower than that of seawater (0.556). Sample 43 is enriched in Ca, K, Li, HCO_3, B and SiO_2 and depleted in Mg and SO_4 with respect to seawater, suggesting extensive seawater-rock interaction and reduction of SO_4.

4.5. Na–Cl waters of medium-high salinity

Medium to high salinity Na–Cl waters discharge from Acqui Terme (samples 1, 6, 6b, 7, 7b, 8, 8b, 48 and 49) and Visone (5, 5b, 15, 15b, 44, 44b, 47) thermal springs and shallow wells. Outlet temperatures are generally significantly higher than average annual air temperature (except for 15, 15b and 49), reaching a maximum of 69.5°C at La Bollente spring (8, 8b). Ionic salinities are 35–85 meq/kg. Silica, Li, K, B, SO_4, F, and Na and Cl are more abundant than in shallow, cold waters. Magnesium and HCO_3 are, on the other hand, less abundant than in cold waters. Calcium is present in comparable concentrations in the Na–Cl, thermal waters and in the cold, Ca–HCO_3 waters.

In the Na vs. Cl plot (Fig. 5A), sample 49 (Acqua Marcia) lies at the saline extreme of an apparent dilution series with the other Na–Cl waters which appear to be mixtures of a saline water with shallow, Cl-poor waters. However, sample 49 has smaller Li and B contents than expected on the basis of the Na–Cl plot, suggesting the uptake of these constituents into secondary minerals (Fig. 5B and C). A similar distribution of samples is also observed in the graphs of K and SiO_2 vs. Cl (Fig. 6A and B), although the samples are more scattered around the dilution line, which in turn is barely recognizable in the diagram of Mg vs. Cl (Fig. 6C). In Fig. 6C, Mg was plotted on a log scale to show the largely variable Mg contents in the Cl-rich thermal waters. The most likely reasons for the scatter of the K, SiO_2, and especially the Mg data, are variable concentrations of these species in cold, Ca–HCO_3 waters and varying reequilibration of mixed Na–Cl waters with rocks at decreasing temperatures (Marini et al., 1998). Immediately after mixing, concentrations

of dissolved chemical constituents in the mixtures are fixed by the mixing process and mixed waters are expected to lie on binary mixing lines in Cl plots. In general, the mixtures will not be in equilibrium with respect to relevant minerals at the T, P_{CO_2}, m_{Cl} conditions fixed by the mixing process, even though the thermal endmember had equilibrium composition prior to mixing. Therefore, the mixtures will react with the enclosing rocks and the concentrations of compatible chemical species will evolve towards the equilibrium value at the T, P_{CO_2}, m_{Cl} conditions fixed by the mixing process (Chiodini et al., 1991). Different mineral-solute subsystems will respond at variable rates to the changes in T, P_{CO_2} and m_{Cl}. However, given enough time, the mixtures will finally reach the new equilibrium compositions. Variable reequilibration of mixed Na–Cl waters with rocks will therefore result in scattered distributions of points in Cl plots.

5. Chemical geothermometry

According to Giggenbach (1988), possible attainment of mineral-solution equilibrium can be identified on the basis of relative Na, K and Mg concentrations. These are conveniently displayed in a Na–K–$Mg^{1/2}$ triangular plot (Fig. 7), also reporting two curves that represent the relative Na, K and Mg contents of geothermal waters in full equilibrium with a thermodynamically stable mineral assemblage (comprising a silica mineral, albite, K-feldspar, illite and chlorite) having the composition of an average crustal rock. Both curves are based on the K–Mg geothermometer of Giggenbach (1988), but on different formulations of the Na–K geothermometer, proposed by Giggenbach (1988, upper curve) and Fournier (1979, lower curve). The samples from the springs of Acqui Terme that contain the largest Cl concentrations (6, 6b, 7, 7b, 8, 8b, 48), except sample 49, plot between the two full equilibrium curves at temperatures of 115–135°C (Fig. 7). Samples 44 and 44b also plot between these two curves but are shifted slightly towards lower temperatures (105–120°C): they mimic a condition of full equilibrium, owing to their anomalously low Mg contents (Fig. 6C), which are likely to be controlled by incorporation of Mg in precipitating calcite (see below). Among the other Na–Cl waters of medium–high salinity, samples 5, 5b, 47, 15 and 15b plot along a trend

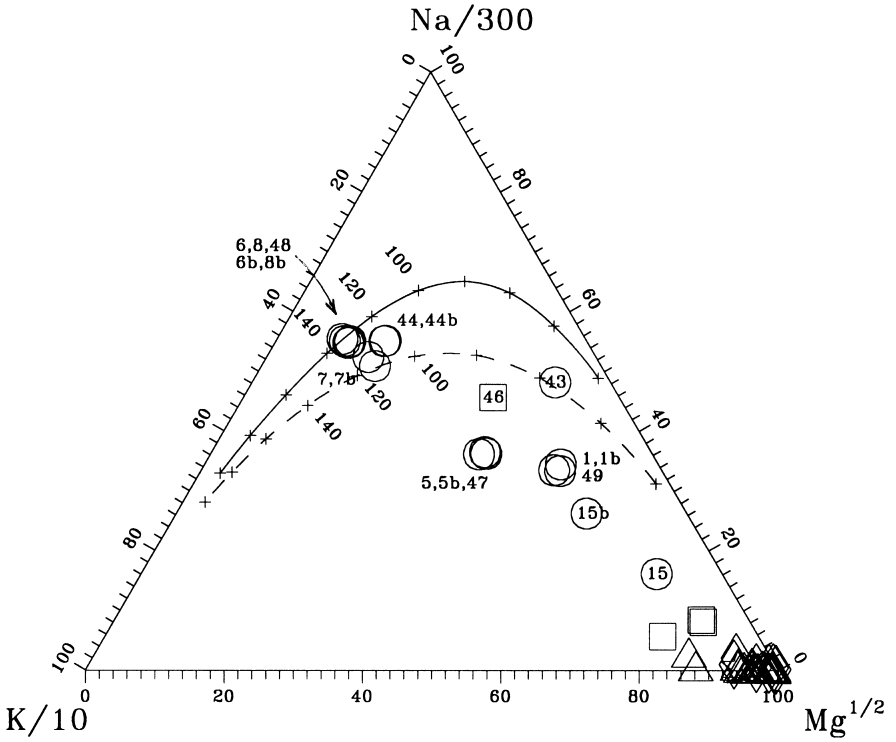

Fig. 7. Na–K–$Mg^{1/2}$ triangular plot (adapted from Giggenbach, 1988). The full equilibrium lines comprise the compositions of waters that have attained equilibrium with the thermodynamically stable mineral assemblage with the composition of an average crustal rock. The solid curve is from Giggenbach (1988); the dashed curve is based on the K–Mg geothermometer of Giggenbach (1988) and the Na–K geothermometer of Fournier (1979). Symbols as in Fig. 3.

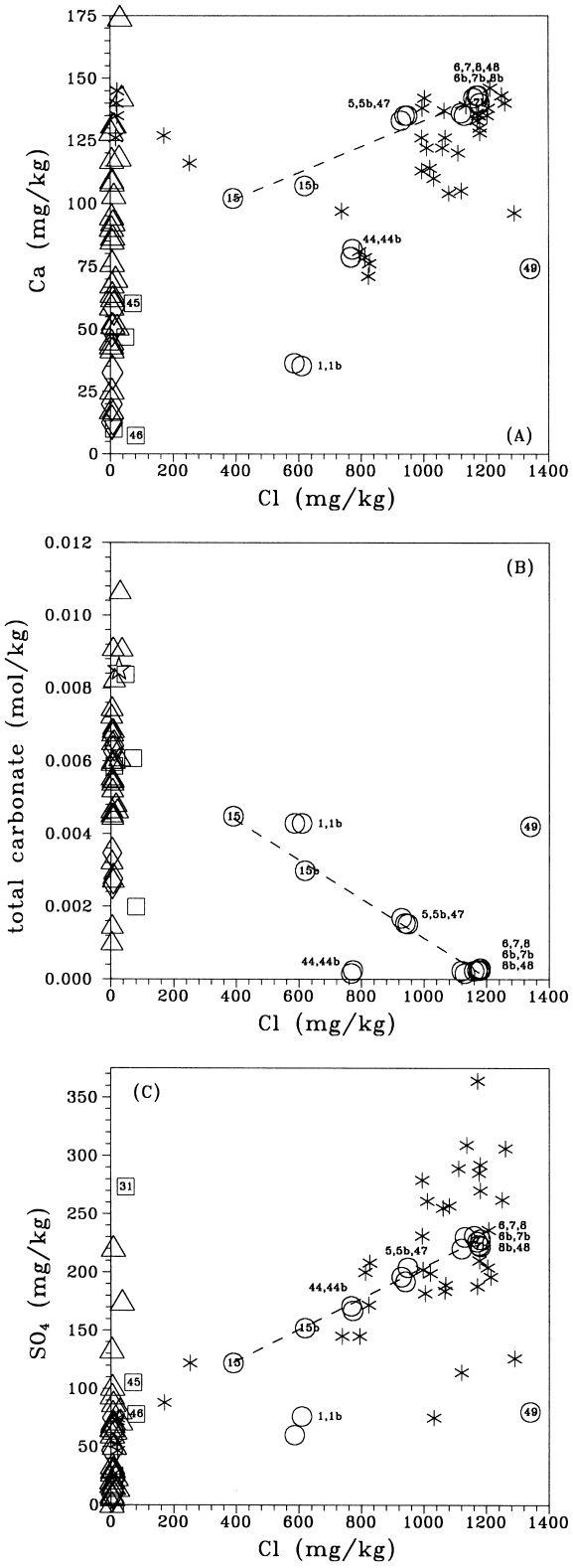

with Na/K ratios similar to those of previous samples, but shifted towards the $Mg^{1/2}$ vertex, apparently owing to mixing with shallow waters and limited water–rock reaction (reequilibration) after mixing. Samples 1, 1b and 49 plot slightly above this trend towards higher Na/K ratios; the discrepancy between their Na–K temperatures (90–110°C) and the K–Mg temperatures (~65°C) could reflect the different rates of readjustment of these two geothermometers with decreasing temperatures; as the K–Mg geothermometer responds faster than the Na–K geothermometer (Giggenbach, 1988), the authors consider the temperature provided by the former to be more representative. Also sample 46 (a Na–HCO_3 water) and sample 43 (a Na–Cl water of high salinity) are close to the low full-equilibrium curve at temperatures of ~80 and 60°C, respectively.

The quartz geothermometer (Fournier and Potter, 1982) provides other indications on the temperatures of mineral-solution equilibrium. Apparent quartz-temperatures are: (a) close to 100–110°C for the springs of Acqui Terme that have the largest Cl concentrations (6, 6b, 7, 7b, 8, 8b, 48), except sample 49; these temperatures are somewhat lower than those suggested by Fig. 7 as the quartz geothermometer is affected by dilution; (b) ~95°C for samples 5, 5b, 47; (c) 70–80°C for samples 1, 1b, 15, 15b, 44, 44b and 49; (d) ~65°C for sample 46 and (e) ~50°C for sample 43.

Summing up, chemical geothermometers suggest the presence, underneath Acqui Terme-Visone, of a main geothermal reservoir at 120–130°C, containing waters in chemical equilibrium with quartz, albite, K-feldspar, illite and chlorite (or smectite). These waters feed most Na–Cl thermal springs of medium–high salinity. Samples 1, 1b and 49 are likely to be connected to secondary reservoirs where the water of the main reservoir, either undiluted or mixed with low-salinity waters, reequilibrates at 65–70°C. Sample 43 (a Na–Cl water of high salinity) probably comes from a separate stagnant aquifer where it spends a long time, sufficient for attainment of mineral-solution equilibrium at 50–60°C. Also sample 46 (a Na–HCO_3 water) comes from a separate aquifer, whose temperature is close to 65–80°C.

Finally, it must be stressed that these equilibrium temperature estimates for the main geothermal reservoir agree with those of Dominco et al. (1980), but are much lower than the 200°C obtained by Bortolami et

Fig. 8. Plots of (A): Ca, (B): total carbonate and (C): SO_4 vs. Cl concentrations for the waters of the study area. Dashed lines refer to the dilution lines of the Na–Cl waters of medium–high salinity. They have been obtained through first-degree linear regression fit for samples 5, 5b, 6, 6b, 7, 7b, 8, 8b, 15, 15b, 47 and 48. Symbols as in Fig. 3.

al. (1983, 1984) through application of unrealistic mixing models.

6. Bacterial sulfate reduction

6.1. Chemical evidence

Further indications of the processes occurring during the ascent of the thermal, Na–Cl waters of medium–high salinity towards the surface are given by the correlation plots of Ca vs. Cl (Fig. 8A), total carbonate vs. Cl (Fig. 8B) and SO_4 vs. Cl (Fig. 8C).

In Fig. 8A, samples 5, 5b, 6, 6b, 7, 7b, 8, 8b, 15, 15b, 47 and 48 plot on the dilution line of the Na–Cl thermal waters, which was identified by means of the Na vs. Cl plot (see above). Samples 1, 1b, 44, 44b and 49 plot below this dilution line, probably because of precipitation of a Ca-bearing mineral, most likely calcite. The saturation indexes of these 5 samples with respect to calcite at outlet conditions, +0.2 to +0.4, are consistent with the occurrence of calcite precipitation.

However, in the total carbonate vs. Cl graph (Fig. 8B), only samples 44 and 44b plot below the dilution line, as expected upon calcite precipitation, whereas samples 1, 1b and 49 are found above this line, indicating a process contributing carbonate, in excess of that subtracted by calcite precipitation. Finally in the SO_4 vs. Cl graph (Fig. 8C), samples 44 and 44b plot on the dilution line (as they are affected by calcite precipitation only), whereas samples 1, 1b and 49 plot below it.

A process that causes a decrease of SO_4 and a concurrent increase of total carbonate, as observed in these 3 samples, is SO_4 reduction, which results in a corresponding increase in total sulfide, either H_2S or HS^- or S^{2-} depending on pH. As a matter of fact, the highest total sulfide concentrations (expressed as HS^-) were found in samples 1 (9 ppm), 1b (17 ppm) and 49 (31 ppm), whereas other thermal, Na–Cl waters of medium–high salinity have total sulfide concentrations of 0.01–2 ppm. Sulfate reduction can be either thermochemical or, most likely, mediated by bacteria.

The thermochemical process is sluggish at temperatures lower than ~140°C (Aplin and Coleman, 1995). Although the occurrence of this nonbiological process is possible, the evidence in favor of bacterial mediation has been growing in recent years. Thermophilic and hyperthermophilic SO_4-reducing bacteria have received considerable attention, mainly because they generate large amounts of H_2S in oil production systems and in oil reservoirs, thus contributing to reservoir souring (e.g., Rosnes et al., 1991; Aplin and Coleman, 1995). Recent studies (e.g., Genthner et al., 1994; Henry et al., 1994; Beeder et al., 1995; Lien and Beeder, 1997) lead to the identification of new SO_4-reducing bacteria and the optimum conditions (temperature, pH, electron and C sources) for their growth. In laboratory experiments, C and electron donors (e.g., formate, acetate, butyrate, lactate, malate, fumarate, succinate, pyruvate, ...) are either totally oxidized to carbonate or incompletely oxidized to intermediate products, such as acetate.

In nature, it seems likely that C and electron donors are fully converted to carbonate due to the action of microbial consortia rather than single species. As sampled waters were not analyzed for organic C species, it is impossible to prove or reject this hypothesis.

However, in all the thermal, Na–Cl waters of medium–high salinity, formate, acetate and propanoate are below detection limits, which are approximately 0.02, 0.02 and 0.03 mg/kg, respectively, in the working conditions of the ion chromatograph used for the analysis of anionic constituents. As the total alkalinity of the sulfide-rich, SO_4-poor samples 1, 1b and 49 ranges from 4.05 to 4.21 meq/kg, the cumulative contribution of formate, acetate and propanoate to titration alkalinity is less than 1.7%, i.e., within analytical uncertainties.

Based on these findings, total conversion of organic substances to carbonate upon bacterial reduction of SO_4 will be assumed in the following discussion.

Bacterial SO_4 reduction has been generally described by the reaction:

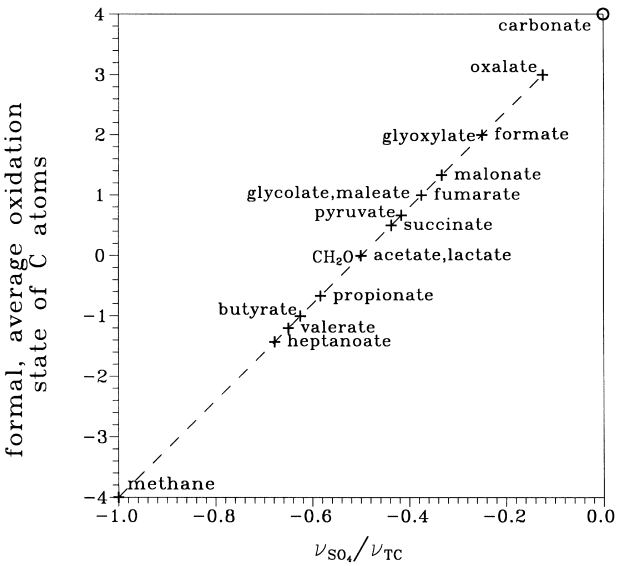

Fig. 9. Relationship between the formal, average oxidation state of C in the organic compounds involved in bacterial SO_4 reduction and the ν_{SO_4}/ν_{TC} ratio.

$$SO_4^{2-} + 2CH_2O = 2HCO_3^- + H_2S, \quad (2)$$

where decomposing organic matter has been schematically represented as CH_2O (e.g., Berner and Berner, 1996; Stumm and Morgan, 1996). The formal oxidation state of the C atom in CH_2O is 0. However, if this process involves organic compounds with nonzero oxidation states of C, instead of CH_2O, its stoichiometry diverges from that of reaction (2). The relationship between the formal oxidation state of C atoms and reaction stoichiometry is (Fig. 9):

$$\langle C \rangle = 4 + 8\,(\nu_{SO_4}/\nu_{TC}) \quad (3)$$

This relationship holds true for any class of organic compounds, and within any given class there is a progressive shift towards the CH_4 point with increasing length of the alkyl chain.

The stoichiometry of bacterial SO_4 reduction in samples 1, 1b and 49 was calculated, by means of simple mass balances, on the basis of the shifts from the dilution trends observed in Fig. 8, assuming that calcite precipitation brings about changes in total carbonate molality which are either equal to the changes in Ca molality (if the system is open to calcite but closed to CO_2) or twice the changes in Ca molality (if the system is open to calcite and CO_2). Calculated ν_{SO4}/ν_{TC} ratios, -0.16 to -0.33, are significantly higher than the ν_{SO_4}/ν_{TC} value of -0.5 implied by reaction (2). It should be noted that if bacterial SO_4 reduction does not involve total conversion of organic substances to carbonate, as assumed in this discussion, ν_{SO_4}/ν_{TC} ratios are higher than calculated.

Based on the relationship between the ν_{SO_4}/ν_{TC} ratio and the formal oxidation state of C (Fig. 9), it can be concluded that the stoichiometry of bacterial SO_4 reduction in samples 1, 1b and 49 implies the involvement of substantially oxidized organic substances, with average oxidation state of C $+1.4$ to $+2.8$. In oil field waters, substantially oxidized organic compounds are largely represented by carboxylate species, especially acetate (up to ~10,000 mg/kg), propanoate (up to ~4400 mg/kg), malonate (up to ~2500 mg/kg), butanoate (up to ~700 mg/kg), and oxalate (up to ~500 mg/kg), (e.g., Dickey et al., 1972; Wiley et al., 1975; Carothers and Kharaka, 1978; Hanor and Workman, 1986; Fisher, 1987; Means and Hubbard, 1987; MacGowan and Surdam, 1990). They originate through either thermal maturation of kerogen (e.g., Carothers and Kharaka, 1978) or hydrolytic bacterial disproportionation of hydrocarbon at the oil–water interface (Helgeson et al., 1993). Carboxylic acids and carboxylate anions might be present also, at depth, in the Acqui Terme-Visone geothermal system and be involved in bacterial SO_4 reduction.

6.2. Isotopic evidence

Samples 6b and 8b have virtually the same $\delta^{34}S$ of dissolved SO_4, at $+38.9$ and $+38.8$‰ vs CDT respectively; a slightly lower value, $+37.7$‰, has been found in sample 44b, whereas sample 1b has a distinctly higher value, $+44.0$‰. The $\delta^{34}S$ of total dissolved sulfide in the latter sample is $+19.4$‰. These data contrast with those obtained by Bortolami et al. (1983, 1984) for La Bollente spring (where we collected sample 8b): $\delta^{34}S_{SO_4} = +17.5$‰; $\delta^{34}S_{H_2S} = -16.3$‰. As the reason for such discrepancy is unknown, only the present data will be discussed.

The $\delta^{34}S_{SO_4}$ of all analyzed samples is remarkably higher than that of any plausible SO_4 source, the most likely of which is Upper Triassic marine sulfate ($+14.6$‰, Nielsen et al., 1991) based on geological considerations (see above). Again, a process that causes an increase in the $\delta^{34}S$ value of residual SO_4, as observed in all the analyzed samples, is bacterial reduction of SO_4 to sulfide, either H_2S or HS^- or S^{2-}, depending on pH (Aplin and Coleman, 1995; Ohmoto and Goldhaber, 1997). It must be stressed that this process takes place not only in samples 1, 1b and 49, as indicated by chemical evidence, but also in samples 6b, 8b, 44b and, most likely, in all the thermal waters of the Acqui Terme-Visone system, as suggested by S isotopes.

Assuming continuous separation of sulfide, through either degassing or precipitation of sulfide minerals, the theoretical evolution of $\delta^{34}S_{SO_4}$ is described by this relationship:

$$\delta^{34}S_{SO4,f} = \delta^{34}S_{SO4,i} + 1000\,(F^{\alpha-1} - 1), \quad (4)$$

where subscripts f and i refer to the final and initial states, respectively, F is the fraction of SO_4 remaining in the system and α is the H_2S-SO_4 fractionation factor (Valley, 1986).

This equation can be used to evaluate F, taking $\delta^{34}S_{SO_4,i} = +14.6$‰, the average isotopic composition of Upper Triassic marine sulfate, and $1000\ln\alpha = -25$‰. This is a typical value for systems closed to SO_4 (Ohmoto and Rye, 1979) and is very close to the $\Delta^{34}S_{H_2S\text{-}SO_4}$ value for sample 1b, -24.6‰. For sample 8b (which has the highest outlet temperature and flow rate) F is 0.39 and the initial SO_4 concentration, before bacterial SO_4 reduction sets in, is 564 mg/kg (analytical SO_4 220 mg/kg).

6.3. Discussion

The saturation index of sample 8b with respect to anhydrite was calculated at varying temperatures by means of the SOLVEQ code (Reed and Spycher, 1984). Sulfate concentration was restored to its initial

value (564 mg/kg) to get rid of the effects of bacterial SO_4 reduction. Since this process brings about variable production of total carbonate, depending on the composition of the organic substances involved as C and electron donors, and this increase in total carbonate is likely to cause precipitation of calcite, it is virtually impossible to recalculate the initial total carbonate and Ca content. Therefore, initial total carbonate was assumed to be fixed by calcite saturation and initial Ca was taken to be constrained by the electric charge balance when running SOLVEQ.

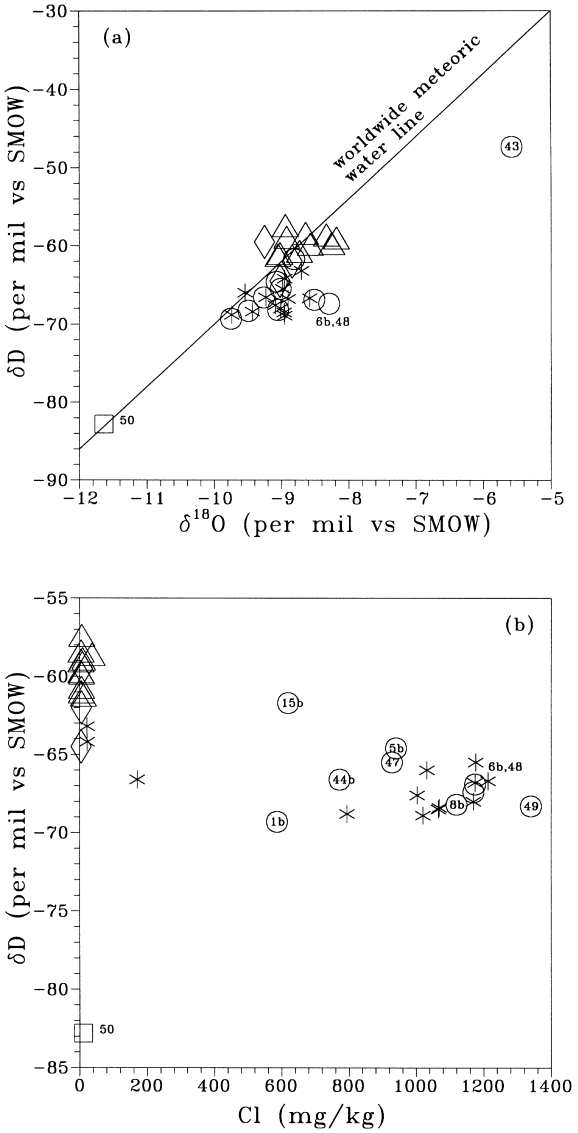

Fig. 10. (A): δD vs. δ^{18}O diagram, showing the isotopic composition of waters sampled in the study area. Also shown is the worldwide meteoric water line. (B): Plot of δD values vs. Cl concentrations.

The saturation index with respect to anhydrite was initially calculated at outlet temperature and measured pH. Temperature was then changed iteratively, keeping the aqueous solution saturated with calcite, and the saturation index recomputed. It turns out that the aqueous solution attains saturation with anhydrite at a temperature of 110°C, which is in good agreement with the equilibrium temperatures given by chemical geothermometers.

The P_{CO_2} value given by SOLVEQ, 0.0105 bar, is very close to the full equilibrium value at 110°C, 0.0117 bar, which is obtained by means of the following equation (Giggenbach, 1988; P_{CO_2} in bar, t in °C):

$$\log P_{CO_2} = 0.0168t - 3.78 \quad (5)$$

According to Giggenbach (1988), Eq. (5) closely describes the temperature dependence of the univariant reaction:

$$\text{Ca-Al-silicate} + \text{K–feldspar} + CO_2 = \text{K–mica} + \text{calcite} \quad (6)$$

Therefore coexisting Ca-Al-silicate and calcite might control P_{CO_2} in the main geothermal reservoir of Aqui Terme.

Summing up, it seems likely that the thermal endmember of Acqui Terme equilibrates with anhydrite in the main geothermal reservoir and bacterial SO_4 reduction takes place within a system that is practically closed to further addition of SO_4 after the thermal water leaves the geothermal reservoir.

Finally it should be noted that occurrence of sulfate reduction in the Acqua Marcia spring (present sample 49) was recognized by Bortolami et al. (1983) on the basis of its relatively high Cl/SO_4 ratio. However it seems unlikely that "the associated generation of reduced sulfur led to the lower pH values observed at this spring with respect to those of the other waterpoints". As indicated by analytical data, sulfide is separated from the aqueous solution as either H_2S gas or mineral sulfides. The pH is instead governed by carbonate species (mainly HCO_3), which are produced through bacterial SO_4 reduction and leave the system through calcite precipitation (see above).

7. δD and δ^{18}O values of water

The δD values of Bortolami et al. (1983, 1984) are higher than in the present study, probably due to an error in standardization or to a systematic instrumental error. This analytical bias was removed by subtracting 5‰ from the δD values of Bortolami et al. (1983, 1984).

In the δD vs. δ^{18}O plot (Fig. 10A) all the waters sampled in the study area, apart from samples 43, 6b, and 48, plot close to the worldwide meteoric water line, indicating a meteoric origin. Sample 50 has an unusually light isotopic composition, suggesting a distinct geographic provenance. This interpretation is reasonable for this sulfide-bearing Na–HCO_3 water, which has a comparatively long circulation time indicated by its chemical composition.

Sample 43, a Na–Cl water of high salinity, plots to the right of the meteoric water line, that is in a position which is typical of other Na–Cl brines of the Po Valley (Bortolami et al., 1984 and references therein) and, in general, of formation waters (e.g., Sheppard, 1986).

Samples 6b (Lago delle Sorgenti) and 48 (Vasca Rotonda) come from two thermal springs discharging Na–Cl waters of medium-high salinity. Both pools have surface areas much larger than other pools, which facilitate evaporation with a large kinetic, diffusion-controlled component (Giggenbach and Stewart, 1982). These peculiar conditions of vapor–liquid separation, rather than dilution of a brine as hypothesized by Bortolami et al. (1983, 1984), are considered to be the cause of the enrichment in heavier isotopes.

Positive ^{18}O-shifts, which are typical of high-temperature, rock-dominated (stagnant) systems (Giggenbach, 1992), are not observed in the thermal waters of Acqui Terme-Visone, in agreement with their provenance from a dynamic, water-dominated system with a rather high natural discharge of ~20 kg/s and temperatures $\leq$120–130°C.

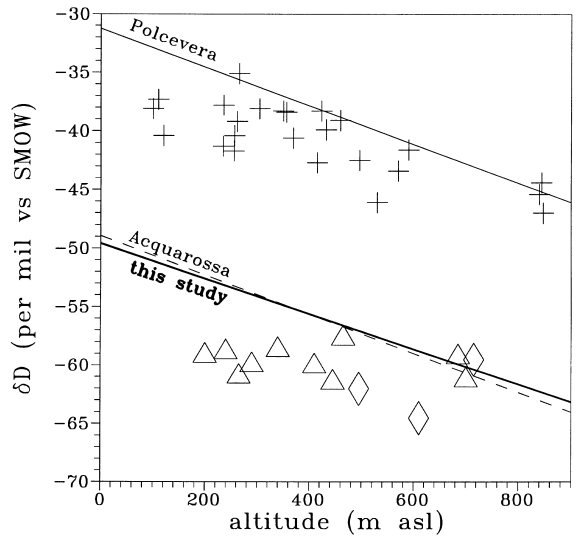

Fig. 11. Plot of δD values vs. altitude of discharge for the cold springs of the study area. Symbols as in Fig. 3. Also shown are values for the cold springs of the Polcevera Valley (Genoa, Italy, from Marini and Ottonello, 1997; crosses) and the δD-altitude relationships for the study area, the Polcevera Valley and the Acquarossa area (Ticino, Switzerland, from Pastorelli et al., 1999; dashed line).

The spread of isotopic properties of the thermal waters in Fig. 10A is also due to mixing of the deep, thermal endmember with shallow, cold waters of different isotopic composition. This process is more evident in the δD vs. Cl plot (Fig. 10B), where the points converge as they approach the thermal endmember, represented by sample 49.

The δD vs. altitude diagram for the cold springs of the study area (Fig. 11) shows that altitude and δD value are strongly correlated. Since it is the discharge altitude rather than the unknown infiltration altitude that is plotted in this diagram, an equation linking the minimum altitude of infiltration of local precipitation (H, m asl) and the δD value can be obtained by drawing a regression line through the points lying to the extreme right, i.e., samples 18, 20, 38 and 39. Such an equation is

$$\delta D = -0.01507 \times H - 49.57 \quad (7)$$

This relationship is very close to that derived by Pastorelli et al. (1999), using the same approach, for the Acquarossa area (Ticino, Switzerland):

$$\delta D = -0.0167 \times H - 48.9 \quad (8)$$

This coincidence is probably fortuitous, at least concerning the intercept. The same exercise leads to the following equation for the springs of the Polcevera Valley, which is located ~20 to 30 km SE of the study area, but on the southern slopes of the Ligurian Alps (Marini and Ottonello, 1997):

$$\delta D = -0.01649 \times H - 31.25 \quad (9)$$

The similarity of the slopes of Eqs. (7)–(9) is not fortuitous and strengthens the validity of this simple technique to link the minimum altitude of infiltration of meteoric waters with their isotopic composition.

Use of Eq. (7) suggests an average recharge altitude of 1200 m asl for the geothermal system of Acqui Terme-Visone, assuming that the thermal endmember is represented by either sample 49 or 8b, whose δD values differ by only 0.1‰ (less than the analytical uncertainty). This altitude value is much higher than the 570–590 m asl proposed by Bortolami et al. (1983, 1984), who used a relationship derived by Bortolami et al. (1979) for the Val Corsaglia, Maritime Alps. Both infiltration altitudes are consistent with the elevations of the Ligurian Alps south of Acqui Terme. However, the large difference between Eqs. (7) and (9), in spite of the comparatively small distance separating these two areas, suggests that the relationships linking the altitude of infiltration of meteoric waters and their iso-

topic composition have to be derived on a very local scale. This is particularly important where orographic barriers, such as the Ligurian Alps, are present. Here, the clouds from the south prevail and experience a first condensation on the southern slopes of the Ligurian Alps, producing comparatively heavy meteoric waters (as in the Polcevera Valley), whereas the precipitations discharging afterwards on the northern slopes of the Ligurian Alps (as in the study area) are isotopically lighter.

8. Tritium

As shown by Bortolami et al. (1983, 1984), ^3H is not detectable in the Na–Cl thermal waters of Acqui Terme-Visone apart from some samples affected by mixing with shallow, ^3H-rich waters. Sample 1b is virtually free of ^3H also.

The mean residence time of ^3H-free waters has been estimated by Marini and Ottonello (1997) using the ^3H data for rain waters collected at the IAEA station of Genoa and the two theoretical models of piston flow and perfect-mixing (Pearson and Truesdell, 1978). Tritium-free waters have mean residence time >42 a according to the first model, and at least some 1000 a based on the second model. These values are somewhat different from those proposed by Bortolami et al. (1984), who presented a misleading log–log plot of ^3H vs. residence time.

9. Geochemical model of the Acqui Terme-Visone geothermal system

The main reservoir of the Acqui Terme-Visone geothermal system has a temperature of 120–130°C and is probably located at a depth of ~3.5 km, assuming a normal geothermal gradient of 33°C/km. This reservoir is fed by meteoric waters infiltrating at an average elevation of ~1200 m asl in the Ligurian Alps, some tens of km south of Acqui Terme-Visone. Meteoric waters move northwards, essentially percolating through and interacting with ophiolites and metasedimentary rocks of the Voltri Group and Mesozoic carbonate-evaporite rocks. In particular, meteoric waters acquire dissolved SO_4 by leaching of Upper Triassic evaporites.

Upon prolonged circulation into the main geothermal reservoir, these waters come to have Na–Cl composition and medium–high salinity and attain chemical equilibrium at 120–130°C with typical hydrothermal minerals including quartz, albite, K-feldspar, illite, chlorite (or smectite), anhydrite, calcite and an unspecified Ca-Al-silicate.

After leaving the zones of the reservoir where Upper Triassic evaporites are present, thermal waters come into contact with oil, acquiring relatively oxidized organic substances, such as carboxylic acids and carboxylate anions, through bacterial disproportionation of hydrocarbons at the oil–water interface.

At this stage of their evolution, the thermal waters are charged with all the substances needed to support the life of SO_4-reducing thermophilic bacteria. These microorganisms reduce SO_4 to sulfide and oxidize organic C to carbonate species, mainly HCO_3, leading to precipitation of calcite. Sulfide is continuously removed from the waters as either gaseous H_2S or mineral sulfides.

In the study area, the impermeable marine sequence of the TPB extends from the surface to depths of 2–3 km, acting as a seal for the geothermal reservoir. In the Acqui Terme-Visone area, this seal is locally weakened by NW- to W-trending normal and strike-slip faults belonging to the transtensive Bagni-Visone fault system (Piana et al., 1997), which creates zones of high vertical permeability. Some thermal waters ascend along these zones and discharge at the surface almost undiluted (e.g., La Bollente, Vasca Rotonda, Lago delle Sorgenti) or mixed with cold, shallow waters (e.g., Caldana di Visone).

To the SW of Acqui Terme, other ascending thermal waters, either undiluted or mixed with low-salinity waters, enter comparatively shallow secondary reservoirs (1.5 km-deep assuming a normal geothermal gradient) and reequilibrate at temperatures of ~65–70°C as indicated by chemical geothermometers. Further bacterial SO_4 reduction takes place in these waters, probably upon addition of further organic matter. Again, the carbonate species produced are partly incorporated into precipitating calcite. The waters escaping from these secondary reservoirs along elements of the transtensive Bagni-Visone fault system either discharge at the surface (Acqua Marcia spring, sample 49) or are tapped at shallow depth (Cassarogna well, samples 1, 1b).

The importance of the transtensive Bagni-Visone fault system is also testified by the presence, near Acqui Terme, of: (1) sulfide-bearing Na–HCO_3 thermal waters, coming from a geothermal aquifer (temperature 70–80°C) located at a depth of ~2 km and (2) Na–Cl brines (Cascina Corsina well) also coming from a relatively hot (50–60°C), deep (1.3 km) aquifer. These waters can also ascend towards the surface along zones of high vertical permeability created by this fault system.

Finally, it must be stressed that, in addition to these secondary occurrences, the Na–Cl thermal waters of medium–high salinity represent, with a deep temperature of 120–130°C, outlet temperatures up to ~70°C and considerable natural discharge (~20 kg/s), a very

interesting geothermal resource, that could be exploited not only therapeutically, as in Roman times, but also for other direct uses. Moreover, the interaction of these thermal waters with oil deserves further studies, for potential economic implications.

Acknowledgements

The paper has received much benefit from the reviews by Professor Stefán Arnórsson and Professor Mark H. Reed to whom we are indebted. The authors are grateful to Professor Everett Shock and Mr. Gavin Chan who gave us appreciated indications on sulfate reduction linked to oxidation of organic substances in hot spring systems, Dr. Luigi Foglino for his friendly support during field work, Dr. Fabrizio Piana and co-workers who made available an early version of their paper on the role of recent tectonics in the study area.

Appendix A. Field characteristics of main thermal and mineral water-points

A.1. La Bollente spring (samples 8, 8b)

The most renowned spring of the Acqui Terme-Visone area is called La Bollente (which is Italian for "the boiling one"), although its outlet temperature is only close to 70°C and no gas bubbles are present. However La Bollente is the hottest spring and has the highest flowrate, ~9 kg/s (Dominco et al., 1980), of the area. It discharges in the centre of Acqui Terme, at 160 m asl, from a neo-classical aedicule that was built in the 19th century.

A.2. Lago delle Sorgenti (sample 6, 6b)

The name of this site is "Lake of the Springs". It is an artificial pond of ~400 m^2, comprising several emergences, located inside the Old Spas. Outlet temperature reaches a maximum of 59.5°C and total flowrate ranges between 5 and 7 kg/s (Dominco et al., 1980). Thermal water discharges are accompanied by gas bubbling. Gas-chromatographic analysis of a sample of this gas, which was collected in February 1997, indicates that it is largely made up of N_2 (98.7 vol%) with some CH_4 (0.56 vol%) and $Ar+O_2$ (0.72 vol%) (Roberto Cioni, personal communication).

A.3. Vasca Rotonda spring (sample 48)

This spring is also located inside the Old Spas and it is bordered by a circular wall of bricks of ~5 m diameter (in Italian "vasca" is tub, and "rotonda" circular). Flowrate is ~3 kg/s and outlet temperature is 42.5°C.

A.4. Cassarogna well (samples 1, 1b)

This artesian well was drilled to a total depth of 147.5 m in 1990. The well head is located at 150 m asl in the south-western outskirts of Acqui Terme. During artesian flow the well has an outlet temperature of ~26°C and flowrate of ~1.2 kg/s. Pumping tests have shown that the outlet temperature reaches ~29.6°C for a flowrate of ~5 kg/s. A TV camera inspection of the well has demonstrated that it is fed by an almost vertical fracture, which is intersected between 126.8 and 128.6 m depths. The maximum width of the fracture is a few cm.

A.5. Cascina Corsina well (sample 43)

This well is located in the alluvial plain of the Bormida river. Its total depth is 65 m. The aqueous solution feeding this well has a temperature of 13.7°C, Na–Cl composition and a very high salinity. Similar brines are not uncommon in these alluvia and were used, especially in war times, to extract salt.

References

Aplin, A.C., Coleman, M.L., 1995. Sour gas and water chemistry of the Bridport Sands reservoir, Wytch Farm, UK. In: Cubitt, J.M., England, W.A. (Eds.), The Geochemistry of Reservoirs, Geological Society Special Publication, 86, pp. 303–314.

Appelo, C.A.J., 1996. Multicomponent ion exchange and chromatography in natural systems. In: Lichtner, P.C., Steefel, C.I., Oelkers, E.H. (Eds.), Reactive Transport in Porous Media, Reviews in Mineralogy, vol. 34, pp. 193–227 (Chap. 4).

Barnes, I., O'Neil, J.R., 1971. The relationship between fluids in some fresh alpine-type ultramafics and possible modern serpentinization, western United States. Geol. Soc. Am. Bull. 80, 1947–1960.

Barnes, I., LaMarche Jr., V.C., Himmelberg, G., 1967. Geochemical evidence of present-day serpentinization. Science 156, 830–832.

Barnes, I., O'Neil, J.R., Trescases, J.J., 1978. Present-day serpentinization in New Caledonia, Oman and Yugoslavia. Geochim. Cosmochim. Acta 42, 144–145.

Beeder, J., Torsvik, T., Lien, T., 1995. *Thermodesulforhabdus norvegicus gentile*. gen. nov., sp. nov., a novel thermophilic sulfate-reducing bacterium from oil field water. Arch. Microbiol. 164, 331–336.

Berner, E.K., Berner, R.A., 1996. Global Environment: Water, Air and Geochemical Cycles. Prentice Hall, Upper Saddle River.

Biella, G.C., Gelati, R., Lozei, A., Rossi, P.M., Tabacco, I., 1988. Sezioni geologiche nella zona limite Alpi occidentali-

Appennino settentrionale ottenute da dati geofisici. Rend. Soc. Geol. Ital. 11, 287–292.

Bortolami, G.C., Cravero, M., Olivero, G.F., Ricci, B., Zuppi, G.M., 1983. Chemical and isotopic measurements of geothermal discharges in the Acqui Terme district, Piemonte, Italy. Geothermics 12, 185–197.

Bortolami, G.C., Olivero, G.F., Zuppi, G.M., 1984. Sistemi idrici profondi, geotermali e freddi, in Piemonte e Valle d'Aosta. Mem. Soc. Geol. Ital. 29, 171–185.

Bortolami, G.C., Ricci, B., Susella, G.F., Zuppi, G.M., 1979. Isotope hydrology of Val Corsaglia, Maritime Alps, Piedmont, Italy. In: Isotope Hydrology 1978, vol. 1. IAEA, Vienna, pp. 327–350.

Cabella, R., Cortesogno, L., Gaggero, L., 1991. Il basamento cristallino del torrente Visone. Rend. Soc. Geol. Ital. 14, 29–33.

Capponi, G., Gosso, G., Scambelluri, M., Siletto, G.B., Tallone, S., 1994. Carta geologico-strutturale del settore centro-meridionale del Gruppo di Voltri (Alpi liguri) e note illustrative. Boll. Soc. Geol. Ital. 133, 383–394.

Carothers, W.W., Kharaka, Y.K., 1978. Aliphatic acid anions in oil field waters: implications for origin of natural gas. AAPG Bull. 62, 2441–2453.

Cassano, E., Anelli, L., Fichera, R., Cappelli, V., 1986. Pianura Padana. Interpretazione integrata di dati geofisici e geologici (Agip). AGIP, San Donato Milanese.

Chiesa, S., Cortesogno, L., Forcella, F., Galli, M., Messiga, B., Pasquarè, G., Pedemonte, G.M., 1975. Assetto strutturale ed interpretazione del Gruppo di Voltri. Boll. Soc. Geol. Ital. 94, 555–581.

Chiodini, G., Cioni, R., Guidi, M., Marini, L., 1991. Chemical geothermometry and geobarometry in hydrothermal aqueous solutions: a theoretical investigation based on a mineral-solution equilibrium model. Geochim. Cosmochim. Acta 55, 2709–2727.

Coplen, T.B., 1988. Normalisation of oxygen and hydrogen isotope data. Chem. Geol., Isot. Geosci. Section 72 (4), 293–297.

Cortesogno, L., Haccard, D., 1984. Carta geologica della zona Sestri-Voltaggio e Note illustrative. Mem. Soc. Geol. Ital. 28, 115–150.

Dickey, P.A., Collins, A.G., Fajardo, M.I., 1972. Chemical composition of deep formation waters in southwestern Louisiana. AAPG Bull. 56, 1530–1533.

Dominco, E., Giraudi, C., Zanella, E., Fancelli, R., Noto, P., Nuti, S., 1980. Le Sorgenti Termali del Piemonte. Regione Piemonte, Assessorato alle Acque Minerali e Termali, Torino.

Ellis, A.J., Mahon, W.A.J., 1977. Chemistry and Geothermal Systems. Academic Press, New York.

Fisher, J.B., 1987. Distribution and occurrence of aliphatic acid anions in deep subsurface waters. Geochim. Cosmochim. Acta 51, 2459–2468.

Fournier, R.O., 1979. A revised equation for the Na/K geothermometer. Geothermal Resources Council Transactions 5, 1–16.

Fournier, R.O., Potter II, R.W., 1982. A revised and expanded silica (quartz)geothermometer. Geotherm. Resources Council Bull. 11, 3–12.

Freeze, R.A., Cherry, J.A., 1979. Groundwater. Prentice Hall, Englewood Cliffs.

Genthner, B.R.S., Mundfrom, G., Devereux, R., 1994. Characterization of *Desulfomicrobium escambium* sp. nov. and proposal to assign *Desulfovibrio desulfuricans* strain Norway 4 to the genus *Desulfomicrobium*. Arch. Microbiol. 161, 215–219.

Giggenbach, W.F., 1988. Geothermal solute equilibria: derivation of Na–K–Mg–Ca geoindicators. Geochim. Cosmochim. Acta 52, 2749–2765.

Giggenbach, W.F. 1992. Isotopic composition of geothermal water and steam discharges. In: D'Amore, F. (Ed.), Application of Geochemistry in Geothermal Reservoir Development. UNITAR-UNDP, Rome, pp. 253–273.

Giggenbach, W.F., Stewart, M.K., 1982. Processes controlling the isotopic composition of steam and water discharges from steam vents and steam-heated pools in geothermal areas. Geothermics 11, 71–80.

Hanor, J.S., Workman, A.L., 1986. Distribution of dissolved volatile fatty acids in some Louisiana oil field brines. Appl. Geochem. 1, 37–46.

Helgeson, H.C., Knox, A.M., Owens, C.E., Shock, E.L., 1993. Petroleum, oil field waters and authigenic mineral assemblages: are they in metastable equilibrium in hydrocarbon reservoirs? Geochim. Cosmochim. Acta 57, 3295–3339.

Henry, E.A., Devereux, R., Maki, J.S., Gilmour, C.C., Woese, C.R., Mandelco, L., Schauder, R., Remsen, C.C., Mitchell, R., 1994. Characterization of a new thermophilic sulfate-reducing bacterium *Thermodesulfovibrio yellowstonii* gen. nov. and sp. nov.: its phylogenetic relationship to *Thermodesulfobacterium Commune* and their origins deep within the bacterial domain. Arch. Microbiol. 161, 62–69.

Lien, T., Beeder, J., 1997. *Desulfobacter vibrioformis* sp. nov., a sulfate reducer from a water–oil separation system. Int. J. Syst. Bacteriol. 47, 1124–1128.

MacGowan, D.B., Surdam, R.C., 1990. Carboxylic acid anions in formation waters. San Joaquin Basin and Louisiana Gulf Coast, USA: implications for clastic diagenesis. Appl. Geochem. 5, 687–701.

Mahon, W.A.J., Klyen, L.E., Rhode, M., 1980. Natural sodium–bicarbonate–sulphate hot waters in geothermal systems. Chinetsu (J. Jpn. Geotherm. Energy Assoc.) 17, 11–24.

Marini, L., Ottonello, G., 1997. Atlante degli Acquiferi del Comune di Genova. I. Alta Val Bisagno ed Alta Val Polcevera. Pacini, Pisa.

Marini, L., Cioni, R., Guidi, M., 1998. Water chemistry of San Marcos area, Guatemala. Geothermics 27, 331–360.

Means, J.L., Hubbard, N., 1987. Short-chain aliphatic acid anions in deep subsurface brines. A review of their origin, occurrence, properties and importance and new data on their distribution and geochemical implications in the Palo Duro Basin, TX. Org. Geochem. 11, 177–191.

Nielsen, H., Pilot, J., Grinenko, L.N., Grinenko, V.A., Lein, A.Yu., Smith, J.W., Pankina, R.G., 1991. Lithospheric sources of sulphur. In: Krouse, H.R., Grinenko, V.A. (Eds.), Stable isotopes: natural and anthropogenic sulphur in the environment-SCOPE 43, vol. 43. Wiley, Chichester, pp. 65–132 (Chap. 4).

Ohmoto, H., Goldhaber, M.B. 1997. Sulfur and carbon isotopes. In: Barnes, H.L. (Ed.), Geochemistry of

Hydrothermal Ore Deposits, 3rd ed. J. Wiley, New York, pp. 517–611 (Chap. 11).

Ohmoto, H., Rye, R.O. 1979. Isotopes of sulfur and carbon. In: Barnes, H.L. (Ed.), Geochemistry of Hydrothermal Ore Deposits, 2nd ed. J. Wiley, New York, pp. 509–567 (Chap. 10).

Pastorelli, S., 1999. Low enthalpy geothermal resources of the Western Alps. Geochemical and isotopic considerations and tectonic constraints. Examples from the Cantons of Ticino and Bern (Switzerland). Ph.D. thesis, Faculty of Sciences, Lausanne Univ.

Pastorelli, S., Marini, L., Hunziker, J.C., 1999. Water chemistry and isotope composition of the Acquarossa thermal system, Ticino, Switzerland. Geothermics 28, 75–93.

Pearson, F.J., Truesdell, A.H., 1978. Tritium in the waters of Yellowstone National Park. US Geological Survey Open-file Report 78–701.

Perello, P., 1997. Interazioni tra strutture tettoniche, fenomeni di sollevamento rapido recente e manifestazioni geotermiche a bassa entalpia nelle Alpi occidentali. Studio di quattro località tipo: Settore Ossolano, Alta Val d'Aosta, Settore Vallesano, Massiccio dell'Argentera. Ph.D. thesis, Dept. Earth Sciences, Turin Univ.

Piana, F., D'Atri, A., Orione, P., 1997. The Visone Formation, a marker of the early Miocene tectonics in the Alto Monferrato domain (Tertiary Piemonte Basin, NW Italy). Mem. Sci. Geol. 49, 145–162.

Reed, M.H., Spycher, N.F., 1984. Calculation of pH and mineral equilibria in hydrothermal waters with application to geothermometry and studies of boiling and dilution. Geochim. Cosmochim. Acta 48, 1479–1492.

Rosnes, J.T., Torsvik, T., Lien, T., 1991. Spore-forming thermophilic sulfate-reducing bacteria isolated from North Sea oil field waters. Appl. Environ. Microbiol. 57, 2302–2307.

Sheppard, S.M.F., 1986. Characterization and isotopic variations in natural waters. In: Valley, J.W., Taylor Jr., H.P., O'Neil, J.R. (Eds.), Stable isotopes in high temperatures geological processes, Reviews in Mineralogy, Vol. 16, pp. 165–183 (Chap. 6).

Stumm, W., Morgan, J.J., 1996. Aquatic chemistry: chemical equilibria and rates in natural waters, 3rd ed. Wiley, New York.

Valley, J.W., 1986. Stable isotope geochemistry of metamorphic rocks. In: Valley, J.W., Taylor Jr., H.P., O'Neil, J.R. (Eds.), Stable Isotopes in High Temperatures Geological Processes, Reviews in Mineralogy, vol. 16, pp. 445–489 (Chap. 13).

Wiley, L.M., Kharaka, Y.K., Presser, T.S., Rapp, J.B., Barnes, I., 1975. Short chain aliphatic acid anions in oil field waters and their contribution to the measured alkalinity. Geochim. Cosmochim. Acta 39, 1707–1711.

Wolery, T., 1992. EQ3NR, A computer program for geochemical aqueous speciation-solubility calculations: theoretical manual, user's guide and related documentation (version 7.0). Report UCRL-MA-110662 PT III. Lawrence Livermore National Laboratory, Livermore.

Wolery, T., Daveler, S.A., 1992. EQ6, A computer program for reaction path modeling of aqueous geochemical systems: Theoretical manual, user's guide, and related documentation (version 7.0). Report UCRL-MA-110662 PT IV. Lawrence Livermore National Laboratory, Livermore.